Measured cathode fall characteristics depending on the diameter of a hydrogen hollow cathode discharge

V Gonzalez-Fernandez[1], K Grützmacher[1], A Steiger[2], C Pérez[1] and M I de la Rosa[1]
[1] Dpto. de Física Teórica, Atómica y Óptica, Universidad de Valladolid, Paseo Belén 7, 47011, Valladolid, Spain
[2] Physikalisch-Technische Bundesanstalt, Abbestr. 2-12, D-10587 Berlin, Germany
E-mail: veronica.gonzalez.fernandez@uva.es

Abstract. In this work Doppler-free two photon optogalvanic spectroscopy is used to measure the electric field strength in the cathode fall region of a hollow cathode discharge, operated in pure hydrogen, via the Stark splitting of the 2S level of atomic hydrogen. The cathode fall characteristics are analysed for various pressures and in a wide range of discharge currents. Tungsten is used as cathode material, because it allows for reliable measurements in a fairly wide range of discharge conditions and because of its minimal sputtering. Two cathode diameters (10 mm and 15 mm) are used to study the dependence of the cathode fall on discharge geometry. The measurements reveal that the cathode fall characteristics are quite independent on the cathode diameter for equal cathode current density; hence the measurements can be used to test one dimensional modelling of the cathode fall region for low pressure hydrogen discharges using e.g. plane parallel electrodes.

1. Introduction

Low densities plasmas generated in different discharge devices for a variety of carrier gases or gas mixtures have been investigated, over several decades, experimentally and theoretically in a wide range of discharge conditions. Many of the studies have been dedicated to noble gases, see for instance [2-8]; however, less research was focussed on pure hydrogen discharges [9-18] and the references therein, because hydrogen plasmas are more complex as they are composed of a variety of neutral and ionized molecules and atoms. The studies [9,10,12] report on modelling of the collisional kinetics of pure hydrogen plasmas used to calculate among others the Hα-emission in order to characterize the cathode region of the plasmas. In [10,12] the authors incorporate an extensive review on experimental data published over decades [19-29]. They also demand for reliable and independent measurements of the local electric field strengths (E-field) in the cathode region missing so far in order to prove discharge modelling. The cathode region is of particularly interest, as the cathode fall determines the fluxes of electrons and ions, their energies distribution and charge densities. We report on independent laser-spectroscopic E-field measurements in the cathode fall of a low pressure steady state pure hydrogen plasma generated in a hollow cathode discharge operated in a wide regime of the abnormal glow with a fully developed cathode fall. The range of our measurements overlaps quite well with the region, were the modelling [10,12] has been tested.

For many years our group has used two laser spectroscopy techniques [30-32] for E-field measurements applied to hydrogen (and isotopes) via the Stark splitting of the 2S level using tuneable single longitudinal mode (SLM) laser radiation. Firstly we demonstrated [30] that two-photon polarization spectroscopy allows determining the E-field strength in the cathode fall region of a HCD operated in deuterium. In a more extended study [31-32] we employed optogalvanic measurement technique. This detection is less complex and perfectly suited for determining local electric field strengths by means of two-photon excitation of the 1S-2S transition followed by subsequent photo-ionization in dc discharges. However, these first measurements demanded for some more deepened analysis and improvements of the detection technique.

Therefore, recently detailed calculations were conducted to determine an important measurement parameter, i.e. the spatial resolution provided by our laser spectroscopic condition [34]. The unique experimental conditions i.e. the SLM laser radiation with smooth temporal pulse shape, and the well-known cross sections for excitation, recombination and ionization of atomic hydrogen, open the possibility to determine the spatial resolution from first principles. The measured laser beam irradiance distribution (spatial resolution: 6.7 µm x 6.7 µm) was employed to integrate the corresponding set of coupled rate equations for the duration of the laser pulse (8 ns with FWHM 2.5 ns) on a 50 ps temporal scale. The results shows in detail the

three-dimensional photo-ionization yield, hence the spatial resolution of optogalvanic detection and the variation of the laser pulse energy allow analysing saturation effects due to depletion. The calculations revealed that our measurements can provide an exceptionally high spatial resolution, because about 80% of the entire signal is created in a measurement volume of 100 µm in diameter and 10 mm length; four times better than estimated before. To maintain the best spatial resolution during an extended long lasting experimental measurement campaign, some important improvements of the laser-spectroscopic set up were necessary, and a continuous control of the laser irradiance present in the measurements volume was included to prevent signal saturation.

Beside the laser spectroscopic details, effort has been spent to improve the HCD itself. In previous works [30-32] the hollow cathode was made of stainless steel and we reported that certain maintenance was required to reduce contamination of the plasma due to sputtered cathode material, which can cause disturbing variations of the discharge voltage drop. In this study we used therefore hollow cathodes made of tungsten, known to result in less sputtering and related degradation. Furthermore a new anode design has contributed to improve the discharge symmetry and the short term stability of the discharge impedance, which is crucial for the background signal in optogalvanic detection. To investigate the influence of the discharge geometry on the cathode fall characteristics, two different diameters (10 and 15 mm) and equal cathode current surface density (ranging from 3.18 mA/cm^2 to 9.55 mA/cm^2) were used.

In this paper we describe the whole experimental arrangement, paying attention to the improvements with respect to previous studies [30-33]. The determination of the local E-field strengths via the Stark-splitting of the 1S-2S transition is explained and the detection limit due to the experimental condition is analysed. The tungsten cathodes allow for a wide experimental range of reliable measurements, facilitating to measure the local E-field down to estimated detection limit (about 0.5 kV/cm). In Section 4 we show the experimental results of this study: the E-field variation vs. distance from the cathode surface for several discharge currents, focussing on the comparison of the cathode fall characteristics for the two cathodes diameters driving the discharge at equal cathode current densities and different pressures. Finally, in Section 5, the measurements are analysed within the frame of an extensive general description and modelling of cathode fall region of low pressure hydrogen discharges [10,12]. We have chosen the comparison according to these authors, because they review an extremely wide range discharge condition and their detailed modelling covers the parameter range of our measurements, i.e. fully developed cathode fall.

2. Experimental arrangement

Measurements were performed in a low pressure pure hydrogen plasma generated in a home-made HCD, operated in abnormal glow-discharge regime. This source provides stationary non-local equilibrium plasma, with low density, low kinetic atomic temperature and E-field strength up to 5 kV/cm close to the cathode surface. The discharge design is basically the same already used in previous work [30-32], i.e. the hollow cathode is placed in between two anodes. However, the anode shape has been modified employing cylindrical cone peaked anodes instead of cylindrical hollow ones, see figure 1. The modification ensures an ideal symmetrical discharge, because the current spot is perfectly centred on the anode peak instead of moving around on an anode ring surface. Therefore, the long and short term stability of the discharge impedance is improved, resulting in a remarkable noise reduction for optogalvanic detection.

Anodes and cathode are inserted in a vacuum seal chamber made of brass, which includes electrical isolation, water cooling, gas inlet and outlet and electrical connections. This layout allows inserting cathodes made of different materials with different inner diameters, and studying the impact of those variations on the discharge conditions. The anodes, made of stainless steel, are kept unchanged for the different cathodes. For end-on laser spectroscopic measurements the anodes have two off axis perforations (see figure 1) providing access to the cathode fall area while maintaining the central cone peak for a stable anode current spot.

In this work we used two tungsten cathodes with inner diameters of 10 mm or 15 mm, and 50 mm length. Tungsten is chosen because its low sputtering rate minimizes the contamination of the hydrogen discharge. The HCD is operated at a constant flow rate of hydrogen (about 10 cm^{3}s^{-1}), entering at one anode and leaving at the opposite one. This device gives excellent single shot sensitivity for optogalvanic detection and a good signal to noise ratio in a wide range of discharge conditions: currents from 50 mA to 300 mA and pressures from 400 Pa to 1350 Pa. The power supply can provide up to 1 A at 2 kV. A resistor (1 kΩ) is used for connecting the grounded cathode, and each anode is also connected via another 1 kΩ resistor, to assure that

each anode carries half of the total current discharge.

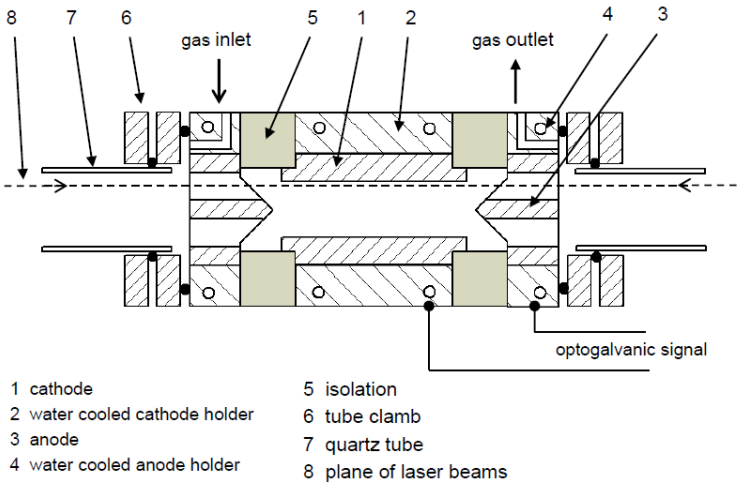

Figure 1: Vertical cross-section of the hollow cathode discharge.

The voltage vs. current characteristic of the HCD is shown in figure 2 for various discharge conditions: pressures from 400 Pa increasing stepwise by a factor 1.5 up to 1350 Pa. Discharge currents varied from 50 mA to 250 mA for a cathode diameter of 10 mm and from 75 mA to 300 mA for a cathode diameter of 15 mm. The interval of equal cathode current densities (j) for both cathode diameters is indicated (arrows) in figure 2, ranging from 3.18 mA/cm^2 to 9.55 mA/cm^2. Those conditions are chosen to study if the E-field in the cathode fall region depends on the cathode diameter, for a fixed current density and pressure. Obviously, for equal current densities the voltage drop for the cathode diameter of 15 mm V_{d15} is systematically larger compared to the voltage drop V_{d10} for a cathode diameter of 10 mm. This might be understood having in consideration that the anode current is increasing by a factor 1.5, while the entire discharge volume is increasing by a factor of 2.25 for the larger cathode diameter. The ratio of the voltage drops V_{d15}/V_{d10} is nearly independent of the current density. Although the long-term stability of the HCD was quite good - including various interchanges of the tungsten cathodes - we have to state that for the entire measurement campaign the discharge voltage V_d was reproducible within ±3% for low currents increasing to ±6% for the highest currents.

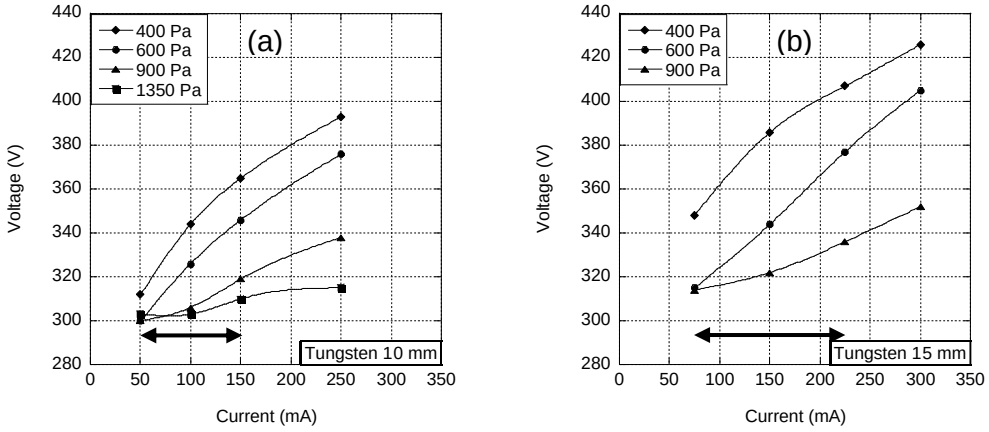

Figure 2: Voltage-Current characteristics for tungsten cathodes (10 and 15 mm inner diameter) for different pressures and currents. The arrows indicate the range of equal cathode current density.

A schematic view of the whole experimental set-up can be seen in figure 3. The laser system consist in a 10 Hz injection-seeded Q-switched Nd:YAG laser (Continuum, Powerlite 9000) and a considerably modified OPO-OPA system (Continuum, Mirage 500). Usually this laser system offers tuneable SLM radiation in the visible and near-IR range (426 nm to 2120 nm). The required 243 nm radiation to excite the 1S-2S transition is obtained by sum-frequency generation (SFG) of 772 nm and the third harmonic (355 nm) from the Nd:YAG in a BBO crystal. This concept can provide up to 10 mJ pulse energy in 2.5 ns and 300 MHz bandwidth. An

etalon having a free spectral range of about 7 GHz and a photodiode (PD) are used to control the regular tuning of the laser frequency by monitoring the OPO signal (772 nm).

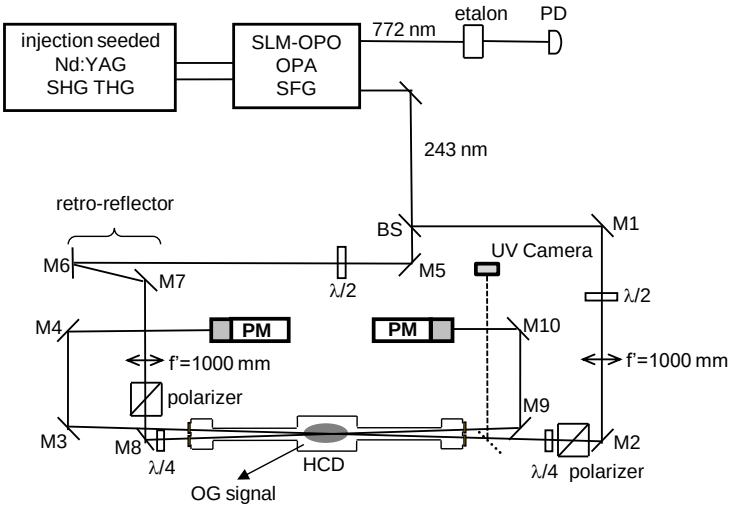

Figure 3: Schematic view of the experimental set-up. The spectra are taken by recording shot by shot the optogalvanic (OG) signal and the references while tuning the laser. The dotted line represents the focus control, by a UV camera, done before and after the measurements.

A moderate amount of the 243 nm laser radiation is introduced in the experiment (figure 3) and divided in two counter propagating beams for Doppler-free measurements. Each beam is focused with a 1 m lens into the plasma, overlapping in a horizontal plane in the upper central part of the HCD, as shown in figure 1. The angle between both beams is very small (1.53°), so that the residual Doppler broadening is negligible compared with the laser bandwidths. The excitation of the 1S-2S transition with an angular momentum transfer $\Delta L = 0$ requires high quality opposite circularly polarized laser beams, provided by high quality air spaced Glan polarizer's followed by zero order $\lambda/4$ retarder plates.

The laser energy of each beam is controlled by a variable attenuator made up of a $\lambda/2$ plate placed before the linear polarizer. In order to avoid saturation and to provide the best signal to noise ratio, the irradiance in the overlap region of the foci of the counter-propagating beams was about 150 MW/cm^2, according to 45 μJ pulse energy. A recent study (see ref [34]) revealed that for these experimental conditions about 80% of the optogalvanic signal corresponds to a measurement volume of only 100 μm in diameter and 10 mm length. Special effort is required to maintain this exceptionally high spatial resolution while tuning the laser frequency, because small variations of the horizontal pointing stability might occur. These would cause that the foci of the counter-propagating beams would suffer an opposite horizontal displacement which may decrease the shot to shot reproducibility of the measurement. This is avoided by installing in one of the beams a horizontal retro-reflector indicated in figure 3. The quality of the focus was controlled twice a day (before and after the measurements) by a spatial profile analyser LaserCam-HR-UV (UV camera in figure 3). Two photomultipliers (PM in figure 3) measure the pulse energy provided by the two beams used to control the shot to shot stability of the laser energy.

The optogalvanic signal is caused by resonant two-photon excitation and subsequent photoionization due to the absorption of a third laser photon. This increases the electron density in the tiny measurement volume, which can be detected as a transient variation of the discharge impedance between the cathode and one anode, via capacitive coupling. To measure the E-field strength through the cathode fall region, the HCD is mounted on two linear translation stages. A vertical displacement of the source allows performing measurements at various distances from the cathode surface. The horizontal displacement is used to align the HCD on the centre axis of the counter-propagating laser beams. For both cathodes the beam divergence and crossing angle are limiting the closest approach of the measurement volume to the cathode surface without irradiating it. Therefore, the measurements start at a distance about 160 μm from the cathode surface. Nevertheless, for a cathode diameter of 15 mm measurements so close to the cathode surface where too noisy, thus these measurements started at a distance of about 260 μm.

3. Measurements and E-field determination

For the E-field measurements, successive laser scans were taken at several distances from the cathode surface for different discharge conditions (pressure, current, cathode diameter). Four signals were simultaneously recorded shot by shot at a repetition rate of 10 Hz in an oscilloscope (Agilent 9000 S-Series), providing an improved data acquisition. Figure 4 shows the quality of the recorded raw data of a typical measurement: (a) it is one of the two photomultipliers signals as reference of the laser energy stability, (b) the optogalvanic signal representing the Stark splitting of the 2S level of hydrogen and (c) transmission of the monitor etalon (fringes) as photodiode signal.

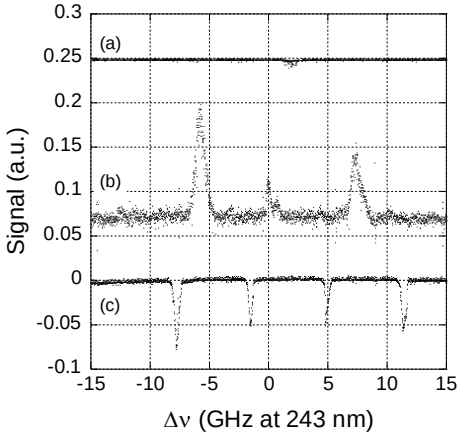

Figure 4: Set of data recorded shot by shot for a typical scan: (a) photomultiplier signal (b) optogalvanic signal of the HCD, (c) transmission of the monitor etalon. The spectrum in (b) was taken at a distance of 350 μm from the cathode surface, in a tungsten cathode of 15 mm inner diameter. The discharge was operated at 400 Pa and 225 mA.

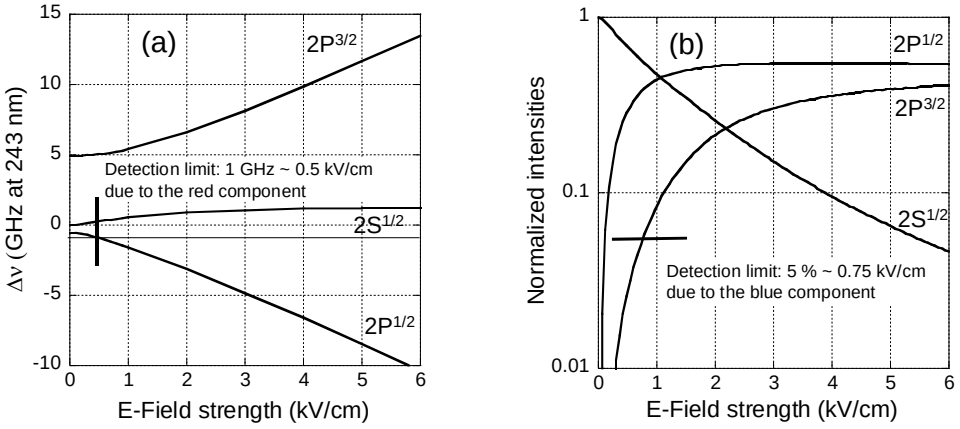

Figure 5: Stark effect of the 1S-2S two photon transition of hydrogen. (a) Shows the calculated frequency shift versus electric field strength. The corresponding two-photon absorption normalized lines intensities are given in (b)

The theoretical Stark splitting of the 2S level as a function of the E-field can be seen in figure 5 [31]. The red shifted component ($2P^{1/2}$) starts to increase strongly near of the central one ($2S^{1/2}$), and suffers a strong and nearly linear displacement if the E-field increases. The blue shifted component ($2P^{3/2}$) starts far off the central one while growing and shifting. The $2S^{1/2}$ component undergoes a weak blue shift and decreases its intensity. The comparison of the experimental spectra with these theoretical predictions allows determining the E-field strength values at different distances from the cathode surface. The detection limit according to the laser bandwidths of 300 MHz and a frequency separation of 1 GHz between the $2S^{1/2}$ and $2P^{1/2}$ components, is estimated to be about 0.5 kV/cm as indicated in figure 5 (a). At this E-field strength, the blue component $2P^{3/2}$ is still too tiny, and an estimated detection limit (5% intensity) corresponds to 0.75 kV/cm, figure 5 (b). However, the spectra recorded close to the cathode surface exhibit good signal to noise ratio and the signals are large compared to the offset. With increasing separation from the cathode surface the E-field strength and

the signal decrease, while the noisy signal offset keeps unchanged. Therefore, the blue shifted component becomes nearly undetectable at E-field strengths below 1 kV/cm depending on the discharge parameters.

To determine frequency differences $\Delta\nu$ between the Stark components, the experimental spectra have been fitted to six Lorentzian profiles, taking into account the hyperfine structure of atomic hydrogen (see figure 6). Therefore, each component in the spectra was fitted to the sum of two Lorentzians with the same spectral width, separated by 621 MHz (for two photon excitation) and an intensity ratio of 3:1. This is done for all spectra, even when the hyperfine structure is not clearly visible. The E-field value is obtained from the difference between the red and blue components (ν_{red}-ν_{blue}) according to figure 5 (a). When the blue component disappears, the difference between the red and central components (ν_{red}-$\nu_{central}$) is used.

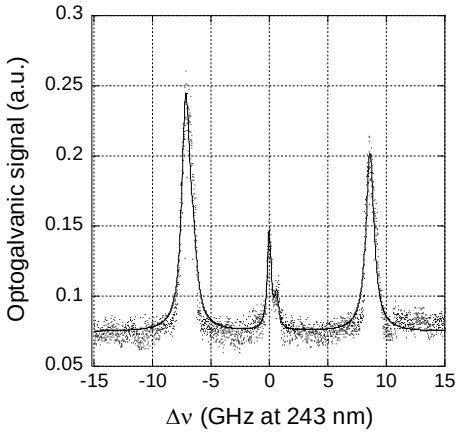

Figure 6: Example of the six Lorentzians fit. The spectrum corresponds to a tungsten cathode diameter of 15 mm, 400 Pa, 300 mA and a distance of 300 μm from the cathode surface. The hyperfine structure can be clearly seen in the central component. The spectrum shows single shot raw data.

In this way, we have determined the local E-field for all spectra measured at different experimental conditions. Figure 7 shows an example of the variation of the E-field versus distance from the cathode surface for a tungsten cathode of 15 mm in diameter, 600 Pa and 150 mA. Each E-field strength value is plotted with the estimated error bar. This estimation is mainly based on the small lack of regularity of the laser frequency tuning, which is controlled via the etalon fringes (see figure 4 (c)). The standard deviation of the fringe separation for the most usual sets of measurements was about 0.16 GHz, half the bandwidth of the laser. Nevertheless, for each plasma conditions particular errors are allotted to each measurement. The uncertainty of the distance from the cathode surface, due to the vertical translator stage position and the alignment procedure, was estimated to 30 μm, which is too small for the axis scale.

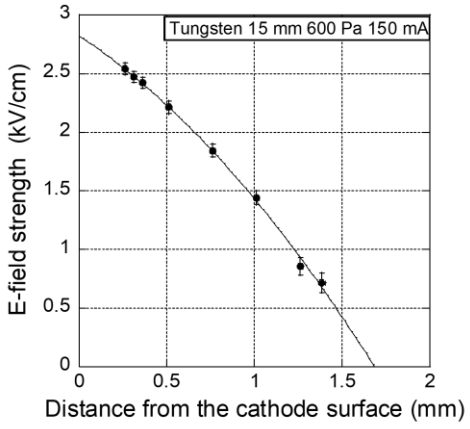

Figure 7: Variation of the E-field versus the radial distance from the cathode surface. Each E-field strength value is plotted with the error bar representing the uncertainty related to the laser frequency tuning.

4. Results

For tungsten cathodes there is a wide experimental range of plasma conditions, where measurements can be

performed with good quality i.e. E-field strength could be determined down to the detection limit, remarkably lower than in previous studies using stainless steel cathodes.

4.1. E-field for various discharge currents for the two cathodes diameters and different pressures.

In figure 8 we show the E-field variation vs. distance from the cathode surface (d) for the two cathode diameters (10 and 15 mm), for several discharge currents and pressures. To keep the same current density (see figure 2), discharge currents are different for the two cathodes diameters. Parabolic or linear fits have been applied to the experimental data. For both diameters and for all pressures the behaviour is very similar: as the current increases the maximum E-field increases while the cathode fall region becomes more compressed and for low currents the cathode fall slope is more linear. Clearly the curves become more compressed with increasing pressure. This is impressively pronounced in the case of the 1350 Pa for the 10 mm diameter, and this tendency is already observed for 900 Pa and the 15 mm diameter. In general, the maximum E-field values are slightly larger for 15 mm diameter, and the cathode fall is more extended.

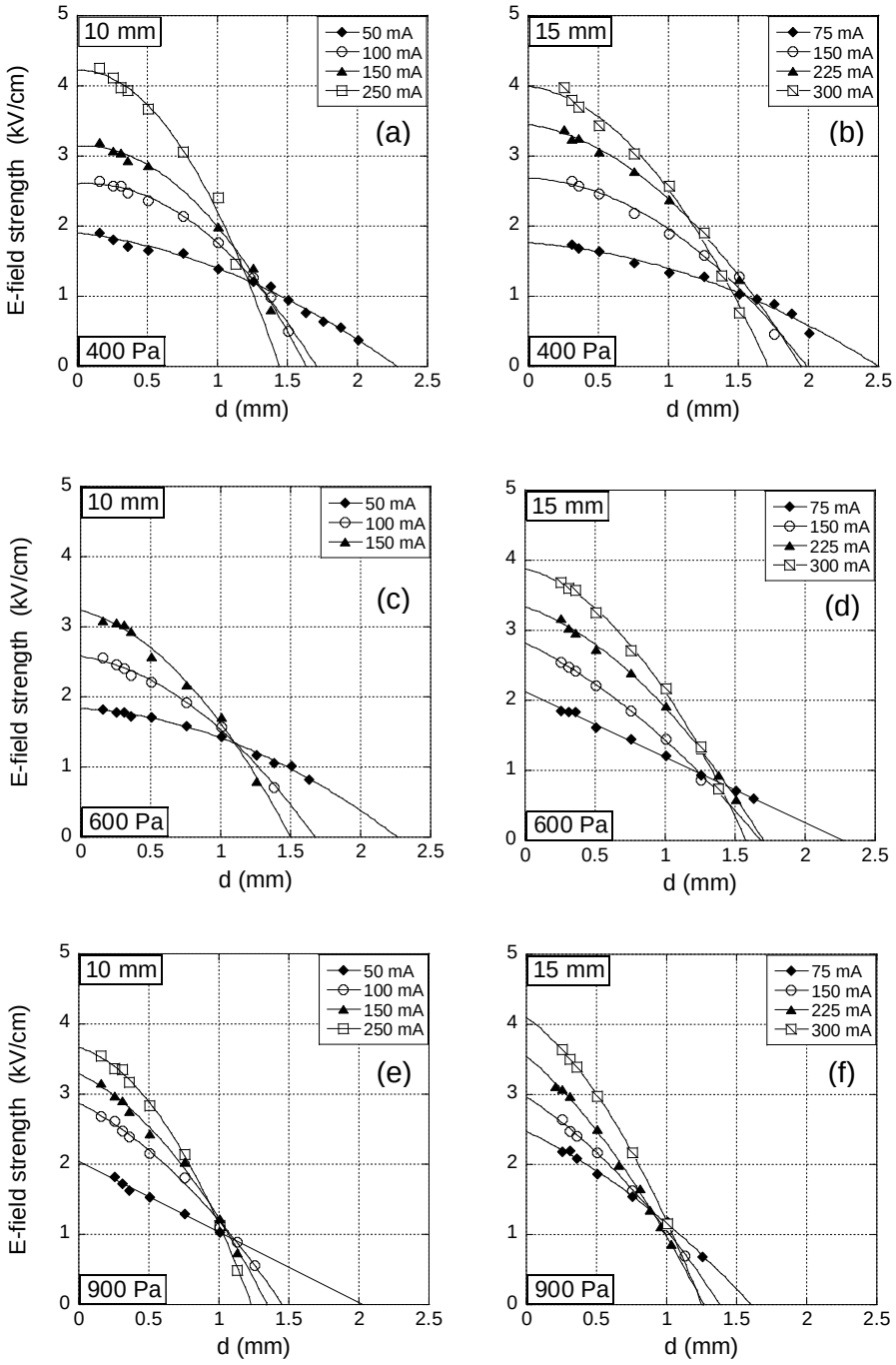

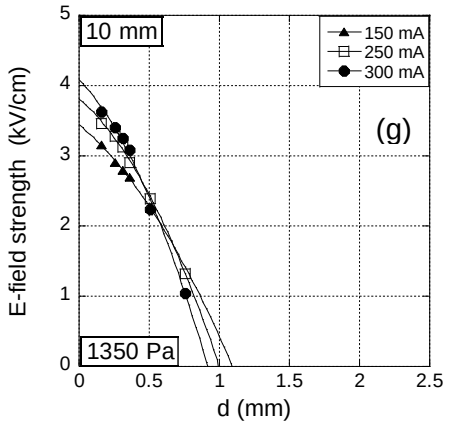

Figure 8: Variation of the E-field in the cathode fall region versus the radial distance from the cathode surface (d), for cathode diameters of 10 and 15 mm and different pressures.

4.2. E-field variation depending on the current densities for the two cathodes diameters and different pressures
Measurements with the same cathode current density for the two cathode diameters at different pressures have been performed to study the influence of the cathode diameter, i.e. the discharge geometry, on the cathode fall characteristics. The corresponding results are given in figure 9. For better clearness, each plot compares only the E-field variation for the two cathode diameters running the discharges at equal cathode current density; discharge currents and pressure are indicated. Plots in one row correspond to the same pressure and plot columns to the same current density.

All plots indicate that for a wide range of discharge conditions the cathode fall is fairly the same for equal current density - i.e. quite independent of the cathode diameter -. Most pronounced differences can be seen at the extreme limits of the discharge conditions e.g. figure 9 (c): lowest pressure and highest current, and figure 9 (g): highest pressure and lowest current. In general, the maximum E-field at the cathode surface increases remarkably with increasing current density. However, the cathode fall changes little with increasing pressure: comparing the plots of the column for current density 6.37 mA/cm^2 for 400, 600 and 900 Pa, we see a slightly increasing maximum E-field at the cathode surface and a corresponding weak compression of the cathode fall toward larger pressure. A certain change of pressure dependence can be observed also: for 400 Pa the cathode fall for the larger currents becomes more separated, and at 900 Pa we see just the opposed tendency. For almost all cases the maximum E-field values are slightly larger for 15 mm diameter (except for the lowest current density at 400 Pa figure 9 (a)), and the cathode fall is more extended.

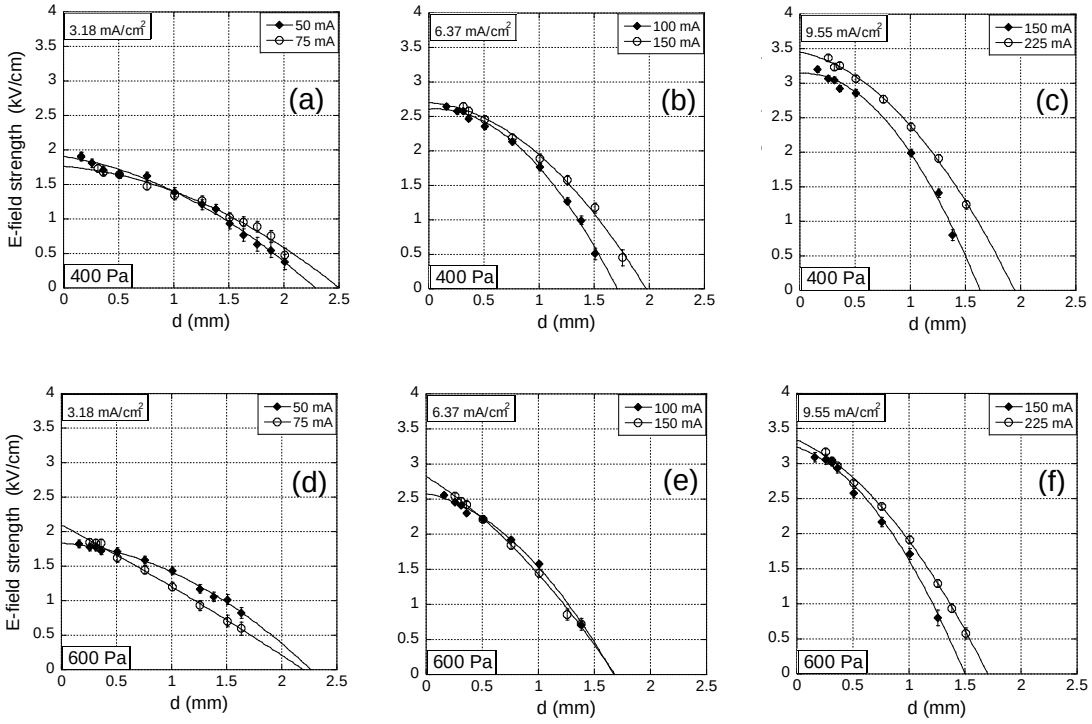

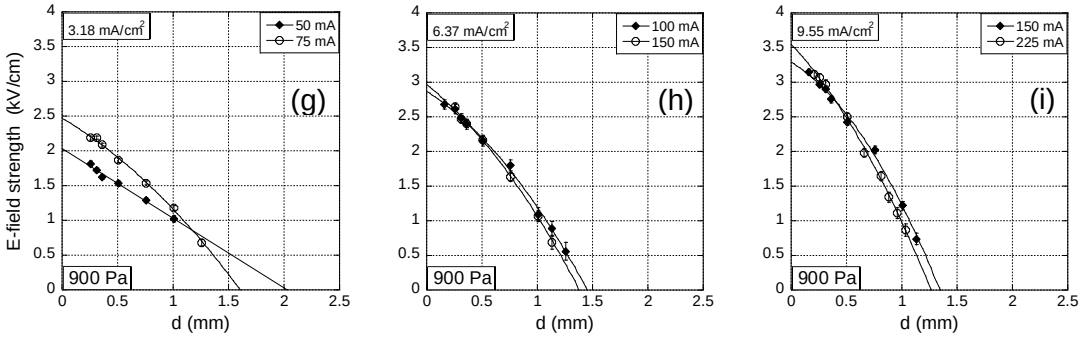

Figure 9: Variation of the E-field in the cathode fall region versus the radial distance from the cathode wall, for cathode diameters of 10 and 15 mm and pressures of 400, 600 and 900 Pa. Graphs shows different current densities (3.18, 6.36 and 9.55 mA/cm^2).

For a quantitative analysis of figure 9 we have integrated the E-field vs. distance from the cathode surface, as this integral corresponds to the entire cathode fall voltage drop V_c. The comparison for the two cathode diameters is provided by the ratio of V_c for equal current density (j) for all discharge conditions, as given in Table 1. This table confirms the apparent impression to be seen in figure 9. For 400 Pa the ratio V_{c10}/V_{c15} is decreasing from 0.96 with increasing current density, for 600 Pa it decreases and varies about 1 ± 0.12 and at 900 Pa it slight increases with increasing current density. Those tendencies are quite insensitive to systematic errors and uncertainties, because all data have been processed in the same way.

Table 1: Ratio of the entire cathode fall voltage drop obtained for the two cathode diameters for equal current density j and all discharge condition.

	400 Pa	600 Pa	900 Pa
j (mA/cm^2)	V_{c10}/V_{c15}	V_{c10}/V_{c15}	V_{c10}/V_{c15}
3.18	0.96	1.12	0.96
6.37	0.87	1.02	0.97
9.55	0.81	0.88	1.05

Further analysis is given in table 2 where the cathode fall voltage V_c is compared with the corresponding entire discharge voltage measured between cathode and anodes V_d (obtained while recording the spectra), for all the experimental conditions in figure 9. The combined uncertainty for those ratios is estimated to be ± 4%. Within our experimental uncertainties the ratio of V_c/V_d is almost the same for a fixed pressure and equal current density Furthermore, this ratio decreases with the pressure and increases with current densities. The smallest ratios are found for 900 Pa at 3.18 mA/cm^2, i.e. cathode fall is representing only the 70% of the discharge voltage, while for the largest current density, 400 Pa and a cathode diameter of 15 mm the cathode fall represents up 97 % of the discharge voltage.

Table 2: Ratio of the cathode fall voltage to the entire discharge voltage, obtained for the two cathode diameters for equal current density j and all discharge condition.

	400 Pa		600 Pa		900 Pa	
j (mA/cm^2)	V_{c10}/V_{d10}	V_{c15}/V_{d15}	V_{c10}/V_{d10}	V_{c15}/V_{d15}	V_{c10}/V_{d10}	V_{c15}/V_{d15}
3.18	0.85	0.86	0.86	0.80	0.71	0.72
6.37	0.88	0.94	0.81	0.79	0.79	0.77
9.55	0.86	0.97	0.84	0.87	0.82	0.78

Comparing Table 1 and Table 2 we can draw a clear conclusion: the cathode fall voltage V_c is nearly independent from the discharge geometry, while the entire discharge voltage V_d depends on the all discharge parameters. This means, that the energy input required for maintaining the plasma in the region from the anode

towards the cathode fall depends definitely on the discharge geometry, and it shows up only in the entire discharge voltage V_d.

5. Comparison with modelling of hydrogen discharges

The analysis presented above demonstrates in fairly good approximation that the cathode fall characteristics measured in this study do not depend on the cathode diameter of the HCD, and we conclude therefore, that they are suited to be compared - particularly - with data obtained from plane parallel electrode geometry [19-23]. Hence our data are valid to test one dimensional modelling of the cathode fall region of low pressure hydrogen discharge. In this way, we have analysed our discharge conditions and related experimental results within the frame of the cathode fall modelling and discharge characterization presented in references [10, 12]. We have chosen the comparison with these articles because they review an extremely wide range of discharge conditions, and their detailed modelling covers the wide parameter range of our measurements. First we present in figure 10 our experimental results in the commonly used format of figure 2 of [12]: voltages versus normalized current density defined as j/p^2 (p being the discharge pressure), in the same units as in [12] for better comparison. Figure 10 gives the cathode fall voltage V_c and also the entire discharge voltage V_d, and we do not distinguish voltages that correspond to cathode diameters of 10 or 15 mm. Clearly our measurements are covering a real wide range of normalized current density, more than one order of magnitude; although the current density varies only by a factor of 3, see Table 2. Comparing the slopes of V_d and V_c one can distinguish more tendencies than in Table 2. For large normalized current densities, - low pressure and large current density - the cathode fall voltage nearly represents the entire discharge voltage drop, confirming the common viewpoint of low pressure discharges. However, this does not hold anymore for decreasing normalized current densities, - towards higher pressure and smaller current density, because maintaining the plasma outside the cathode fall requires additional energy. The open cross in figure 10 corresponds the main result given in reference [12], obtained from measurements (2 Torr, 327 V and 55 mA) and modelling, which fits perfectly with our V_d values, and is only a little bit larger than our cathode voltage drop values.

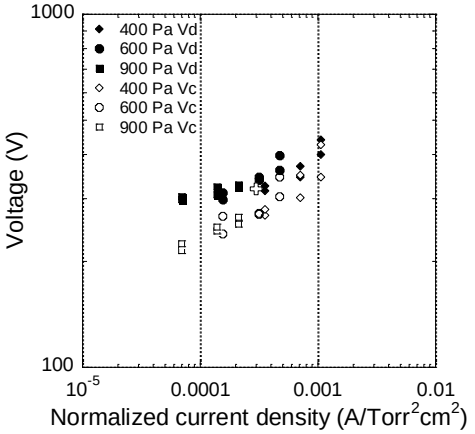

Figure 10: Cathode fall voltage V_c (open dots) and the entire discharge voltage V_d (full dots) versus normalized current density. The open cross corresponds to the main result (2 Torr, 327 V and 55 mA) given in [12].

We have also plotted the normalized thickness of the cathode fall pd_{cf} (pressure p times cathode fall thickness d_{cf}) versus normalized current density in figure 11 (same representation as in figure 2 of ref. [12]). Once more, the open cross in figure 11, which corresponds to the main result given in reference [12], fits perfectly with our measurements.

The good agreements with reference [12] confirms our former conclusion that the cathode fall characteristics measured in this study do not depend on the cathode diameter of the HCD and that the normalized current density is a very useful parameter that opens the possibility to compare different discharge condition.

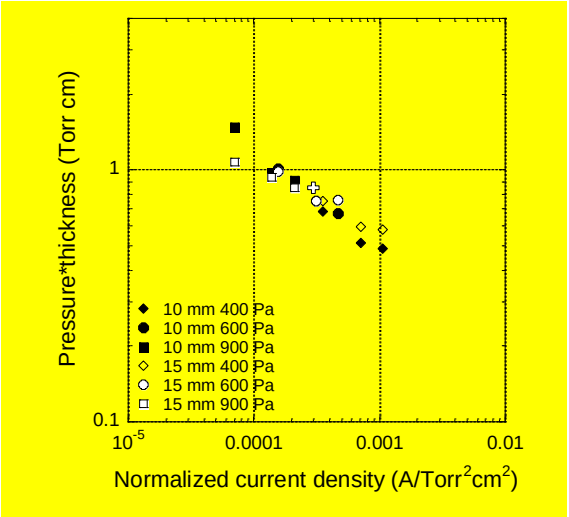

Figure 11: Normalized thickness of the cathode fall pd_{cf} (pressure p times cathode fall thickness d_{cf}) versus normalized current density. The open cross corresponds to the main result (2 Torr, 327 V and 55 mA) given in [12].

We have represented also our data in the frame described in the Topical Review [10]. This frame is quite general, as it is proposed to yield for all type of discharge geometries commonly used for plane parallel electrodes and hollow cathodes as well. Figure 12 shows some measured E-field strength obtained in this work using the same units as in figure 2 of ref. [10], i.e. the E-field strength to gas density in Townsed (1 Td = 10^{-21} Vm^2) vs. gas pressure times distance to the cathode surface. The results are only plotted for 15 mm cathode diameter as they are basically the same as for 10 mm diameter. Figure 12 (a) represents selected discharge conditions showing, that low discharge currents at low pressures correspond to a similar slope as higher currents at higher pressures. Hence, although the E-field strength for 900 Pa - 225 mA is considerably higher than for 400 Pa - 75 mA (see figure 8), the data in figure 12 (a) become quite similar due to the normalization by the gas density N. This behaviour is reversed when contrary conditions are plotted: 400 Pa at 225 mA achieves higher values than 900 Pa at 75 mA. We can provide experimental data in a wide range for theoretical analysis. That means the E-field strength measured in our HCD can be directly compared with very different electrodes discharge geometry [22-25] presented in reference [10].

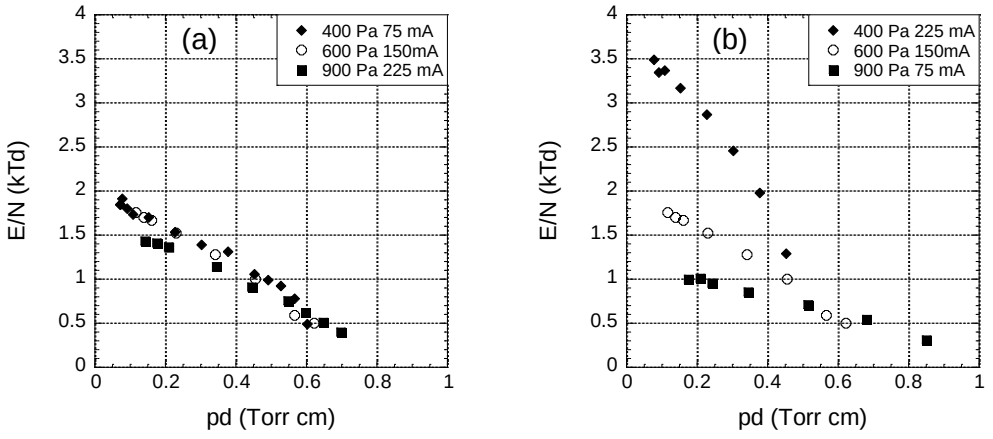

Figure 12: Measured E-field strength to gas density in kTd (10^3 Td) vs gas pressure times distance to the cathode surface, in a 15 mm cathode diameter. Different plasma conditions are presented in figures (a) and (b).

Finally, in figure 13 the E-field strength to gas density vs. current density in A/m^2 is plotted, in the same scale as figure 3 in ref. [10]. Only the data for 15 mm cathode diameter are shown. The right side of the solid line in figure 13 correspond [10] to experimental conditions of sufficiently large electrode separations and current densities expected to be required for a fully developed cathode fall. Our extensive and detailed measurements cover a wide part of that area, and are - to our knowledge - the only ones which really represent highly resolved local electric field strength of the cathode fall, compared with various experimental studies which provide merely average values [9, 13, 22-29] compiled in [10].

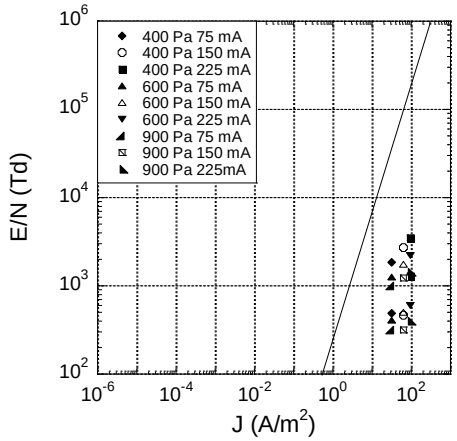

Figure 13: Measured E-field strength to gas density in Td units vs current density for the 15 mm cathode diameter. The right side of the solid line corresponds to a fully developed cathode fall.

6. Summary

In this paper, we report E-field measurements in tungsten cathodes with two different diameters in a HCD operating in pure hydrogen. The E-field was determined via Stark splitting of the 2S level of hydrogen, based in Doppler-free two-photon absorption provided by two counter-propagating circularly polarized beams of opposite directions. Optogalvanic detection, i.e. changes of the plasma impedance caused by the resonant excitation of the 2S level and subsequent photo-ionization by a third photon were recorded by capacitive coupling to obtain the spectra. The E-field is determined by measuring the frequency shift between the red ($2P^{1/2}$) and the blue ($2P^{3/2}$) components. A UV laser spectrometer provides the required high-power single-longitudinal mode and tuneable 243 nm radiation with 2.5 ns temporal duration and 300 MHz bandwidth.

The redesigned plasma source provides remarkably improved long and short time stability of the discharge using tungsten cathodes and newly designed stainless steel anodes. Together with important improvements of the laser-spectroscopic the experimental set-up allows extended spectroscopic measurements with exceptional high spatial resolution (100 µm in diameter and 10 mm length) in a wide experimental range. Compared with previous works, we could realize measurements down to the estimated detection limit given by the Stark splitting of 2S level, i.eg. E-field strength of 0.5 kV/cm.

The E-field measurements were performed for pressures varying from 400 Pa to 1350 Pa and for currents from 50 to 300 mA. Measurements were conducted in a fairly wide range of discharge conditions for three values of equal current density for both tungsten cathode diameters (10 and 15 mm), revealing the influence of the cathode diameter on the cathode fall characteristics. Certain tendencies can be observed; also the cathode fall does not change significantly. More pronounced differences were found for extreme discharge conditions: low pressure and high current and the opposite, high pressure and low current.

We can conclude in fairly good approximation, that the cathode fall characteristics measured in this study do not depend on the cathode diameter of the HCD, and it is demonstrated, that they are well suited to be compared with experimental data and indirect determination of cathode fall voltage obtained from or for quite different electrodes discharge geometry. Our extensive and detailed measurements cover a wide and representative interval of low pressure discharge conditions, and so they are valid to test one dimensional modelling of the cathode fall region of low pressure hydrogen discharges.

This experimental work can be completed with a study of the influence of the buffer gas. The same experimental device can be employed to perform E-field measurements in hydrogen isotopes, with a tiny change in the scanning wavelength.

Acknowledgments

The authors thank DGICYT (Ministerio de Economía y Competitividad) for the project ENE2012-35902, FEDER funds and the grants BES-2013-063248 and EEBB-I-16-10654 given to V. González-Fernández. The

authors thank A. Martín and S. González for the technological support, J. L. Nieto for the informatics assistance, E. M. Domingo for the administrative work and A. Steiger for the scientific discussions.

References

[1] Samukawa S et al. 2012 *J. of Phys. D: Appl. Phys*. **45** 253001
[2] Gavrilenko V P, Kim H J, Ikutake T, Kim J B, Choi Y W, Bowden M D and Muraoka K 2000 *Phys. Rev. E* **62**, 5, 7201
[3] Bogaerst A, Chem z and Gijbels R 2003 *Surf. Interface Anal.* **35** 593
[4] Baguer N, Bogaerts A, Donko Z, Gijbels R and Sadeghi N 2005 *J. of Phys. D: Appl. Phys*. **97** 123305
[5] Donko Z 2011 *Plasma Sources Sci. Technol.* **20** 024001
[6] Phelps A V 2011 *Plasma Sources Sci. Technol*. **10** (2) 329-343
[7] Jiang T, Bowden M D, Wagenaars E, Stoffels E and Kroesen G M W 2006 *New Journal of Physics* **8** 202
[8] Den Hartog E A, Doughty D A and Lawler J E 1988 *Phys. Rev. A* **38** 2471
[9] Phelps A V 2009 *Phys. Rev.* E **79** 066401
Phelps A V 2010 *Phys. Rev.* E **81** 029903
[10] Phelps A V 2011 *Plasma Sources Sci. Technol*. **20** 043011
[11] Jelenković B M and Phelps A V 1996 *Phys. Rev. E* **53** (2) 1852
[12] Jelenković B M and Phelps A V 2011 *Phys. Plasmas* **18** 103505
[13] Gemisic Adamov M, Obradovic B M, Kuraica M M and Konjević N 2003 *IEEE Transactions on Plasma Science,* **31** (3) 444-454.
[14] Gemisic Adamov M, Steiger A, Grützmacher K and Seidel J 2007 *Phys. Rev. A* **75** 013409
[15] Spasojević D J, Steflekova V, Šišović N M and Konjević N 2012 *Plasma Sources Sci. Technol.* **21** (2) 025006
[16] Spasojević D J, Steflekova V, Šišović N M and Konjević N 2014 *Plasma Sources Sci. Technol.* **23** (1) 012004
[17] Spasojević D J, Mijin S, Šišović N M and Konjević N 2016 *J. Appl. Phys*. **119**, 053301
[18] Jiménez-Redondo M, Carrasco E, Herrero V J and Tanarro I 2015 *Plasma Sources Sci. Technol.* **24** 015029
[19] Güntherschulze A 1928 *Z. Phys*. **49** 473
[20] Güntherschulze A 1930 *Zeitschrift für Physik A Hadrons and Nuclei* **59** (7) 433-445
[21] Warren R 1955 *Phys. Rev*. **98** 1650
[22] Barbeau C and Jolly J 1990 *Appl. Phys. Lett.* **58** 237
[23] Cvetanović N, Kuraica M M and Konjević N 2005 *J. Appl. Phys.* **97** 033302
[24] Ganguly B N and Garscadden A 1991 *J. Appl. Phys.* **70** 621
[25] Dexter A C, Farrel T and Lees M I 1989 *J. Phys. D* **22** 413
[26] Lavrov B P and Mel'nikov A S 1995 *Opt. Spektrosc.* **79** 922
Lavrov B P and Mel'nikov A S 1995 *Opt. Spectrosc.* **79** 842 (Engl. Transl.)
[27] Kipritidis J, Khachan J, Fitzgerald M and Shrier O 2008 *Phys. Rev.* E **77** 066405
[28] Petrović Z Lj and Phelps A V 2009 *Phys. Rev.* E **80** 016408
[29] Petrović Z Lj and Phelps A V 2009 *Phys. Rev.* E **80** 066401
[30] de la Rosa M I, Pérez C, Grützmacher K Gonzalo A B and Steiger A, 2006 *Plasma Sources Sci. Technol.* **15** 105-111
[31] de la Rosa M I, Pérez C, Grützmacher K and Fuentes L M 2009 *Plasma Sources Sci. Technol.* **18** 015012
[32] Pérez C, de la Rosa M I and Grützmacher K 2010 *Eur. Phys. J. D.* **56** 369-375
[33] Gonzalez-Fernandez V, Grützmacher K, Fuentes L M, Pérez C and de la Rosa M I 2017 *Journal of Physics: Conf. Series* **810** 012015
[34] García-Lechuga M, Fuentes M, Grützmacher K, Pérez C and de la Rosa M I 2014 *J. Appl. Phys.* **116** 133103